Porous compaction in transient creep regime and implications for melt, petroleum, and CO 2 circulation

B Chauveau, E Kaminski

Porous compaction in transient creep regime and implications for melt, petroleum, and CO_2 circulation

B. Chauveau[1] and E. Kaminski[1]

Received 3 April 2007; revised 4 March 2008; accepted 6 June 2008; published 12 September 2008.

[1] Liquid segregation through a porous medium depends on the ability of the matrix to deform and compact. Earth's materials have a complex rheology, in which the balance between the elastic and viscous contribution to the deformation is time-dependent. In this paper, we propose a Burger-type model to investigate the implications of transient rheology for viscous compaction of a porous material. The model is characterized by three dimensionless parameters: (1) the Deborah number, De, defined as the ratio of an elastic timescale over the compaction timescale, (2) the ratio of the transient and steady viscosities, λ_μ, and (3) the ratio of the transient and steady elastic moduli, λ_G. For $De < 10^{-2}$ the compaction occurs in the classic viscous mode, and solitary waves (magmons) are generated. For larger De, compaction is mainly controlled by λ_μ. For small transient viscosity, compaction occurs in an elastic mode, and shock waves are generated. For increasing λ_μ, two new regimes are observed, first "shaggy" shock waves and then "polytons". Shaggy shock waves are characterized by the presence of secondary peaks at the wave propagation front. The length scale of the peaks is a decreasing function of λ_G, and their amplitude decreases along the propagation. In the polytons regime, the peaks tend to detach and mimic the behavior of solitary waves. Polytons and shaggy shock waves are expected both in the mantle and in sedimentary basins. Polytons will require a particular attention as they imply larger extraction velocities and smaller compaction length scales than the usual magmons.

Citation: Chauveau, B., and E. Kaminski (2008), Porous compaction in transient creep regime and implications for melt, petroleum, and CO_2 circulation, *J. Geophys. Res.*, *113*, B09406, doi:10.1029/2007JB005088.

1. Introduction

[2] A knowledge of the physical parameters controlling the distribution and the transport of liquid in the Earth is necessary to quantitatively model many key geological processes. For example, the amount of liquid in a given rock will modify its physical properties, like its electrical properties [*Revil*, 2002a], especially during deformation [*Hirth and Kohlstedt*, 1995], thermal convection [*Ito et al.*, 1999], or even seismic wave propagation [*Cooper*, 2002; *Kaminski*, 2006]. The amount of liquid depends both on the efficiency of the processes that generate the liquid (melting, diagenesis) and on the characteristics of the transport phenomenon. The efficiency of the transport depends on the pressure gradient and on the permeability, which itself is a function of porosity. Porous flows are encountered in various geological environments, such as core formation [e.g., *Yoshino et al.*, 2003], melt extraction from the convective mantle [e.g., *Spiegelman and McKenzie*, 1987; *Ribe*, 1987; *Scott*, 1988; *Schmeling*, 2006], or fluid maturation and migration in sedimentary basins [e.g., *Connolly and Podladchikov*, 1998; *Yang*, 2000; *Suetnova and Vasseur*, 2000]. These various examples share a common physical framework in which the circulation of a low-viscosity fluid is controlled by the behavior of a more or less deformable matrix. The description of the effective rheology of the porous matrix remains an open question in the modeling of porous flows.

[3] The corner stone of the theoretical setting for two-phase flow has been laid by *McKenzie* [1984], who studied melt extraction from the mantle using a viscous rheology for the matrix. Latter studies focused on the various modes of extraction and showed that solitary waves (magmons) can propagate through a visco-porous matrix [e.g., *Scott and Stevenson*, 1984; *Barcilon and Richter*, 1986; *Spiegelman*, 1993a]. More recent studies have focused on the characteristics of the viscous waves, as a function of the porosity dependence of shear viscosity [*Khodakovskii and Rabinowicz*, 1998], or as a function of surface tension effects [*Bercovici et al.*, 2001; *Ricard et al.*, 2001].

[4] When used to model compaction in sedimentary basins, which occurs on shorter timescales, the two-phase flow theory must include viscoelastic effects [e.g., *Suetnova and Vasseur*, 2000]. Viscoelastic rheology has also been taken into account to study potential elastic effects associated with mantle compaction [*Connolly and Podladchikov*, 1998; *Vassilyev et al.*, 1998; *Kaus and Podladchikov*, 2006] or with seismic wave propagation [*Saenger et al.*, 2005]. These models rely on a description of the viscoelastic

[1]Équipe de Dynamique des Fluides Géologiques, Institut de Physique du Globe de Paris and Université Paris-Diderot, CNRS, Paris, France.

0148-0227/08/2007JB005088$09.00

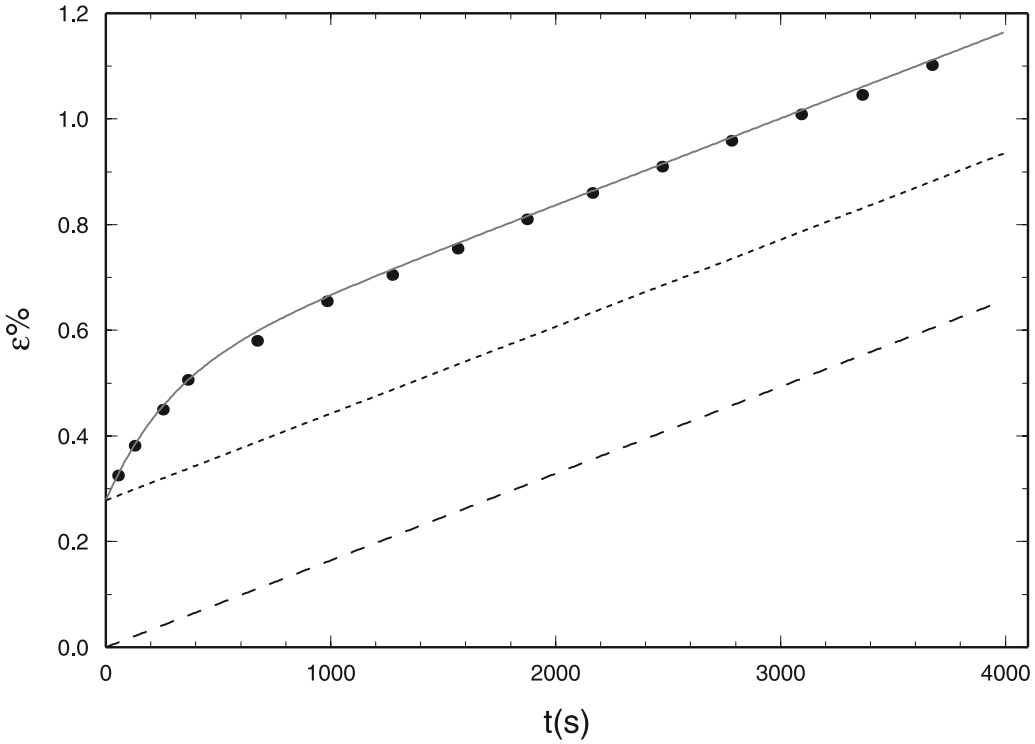

Figure 1. Creep curve of an olivine rock from a laboratory experiment of *Chopra* [1997] (plain circles). The thick line is obtained from the transient creep strain equation (2). The long-dashed line corresponds to a viscous material, and the short-dashed line corresponds to a Maxwell body for the same steady viscosity and elastic modulus. None of these two cases are able to reproduce transient creep.

rheology based on a Maxwell body. A Maxwell body is characterized by a viscosity and by an elastic modulus, the ratio of which defines an elastic timescale [*Joseph*, 1990]. If the timescale of the viscous compaction is much larger than the elastic timescale, elastic effects are negligible and solitary waves, or magmons, are generated [*Connolly and Podladchikov*, 1998]. On the other hand, when the two timescales are close one to another, elastic effects become dominant and the liquid is extracted by shock waves [*Connolly and Podladchikov*, 1998]. These shock waves stay attached to their source region and present a sharp porosity reduction at the propagation front. This regime is likely to occur in sedimentary basins rather than in deep-Earth environments.

[5] A Maxwell body is only a first-order description of viscoelastic rheologies that does not encompass all the characteristics of deformation of Earth materials. Plastic deformation in laboratory experiments is actually described in term of "transient creep" divided into three stages [*Post*, 1977]. Under constant stress, the material first sustains an instantaneous elastic deformation, then its strain rate continuously decreases (transient visco-elastic response) until it reaches a constant value (steady viscous response). A Newtonian material will display the third steady state regime only, whereas a Maxwell body will display both the first (elastic) and third (viscous) responses. None of these two rheologies is able to reproduce the transient stage. As liquid circulation through a deformable matrix is associated with transient deformations, this intermediate regime is, however, potentially relevant. In this article, we will present a systematic study of the behavior of a visco-elastic matrix during its compaction in transient creep regime, and discuss its implications for melt, petroleum, and CO_2 circulation in the Earth.

2. Transient Creep of Visco-Elastic Materials

[6] Laboratory tests performed under controlled conditions, have been used to study transient rheology [e.g., *Post*, 1977; *Carter and Kirby*, 1978]. In high-temperature creep experiments under constant stress, the sample sustains first an instantaneous recoverable strain, followed by a plastic nonrecoverable deformation. The rate of plastic deformation decreases continuously through a so-called transient regime until a steady state regime is reached (Figure 1). The total strain ε (t) can be described by the following kind of relationship [*Andrade*, 1910; *Garofalo*, 1965; *Post*, 1977; *Carter and Kirby*, 1978]

$$\epsilon(t) = \epsilon_0 + \dot{\epsilon}_s \times t + \epsilon_T f\left(\frac{t}{t_r}\right) \tag{1}$$

where ε_0 is the instantaneous strain, $\dot{\varepsilon}_s$ is the steady state strain rate, and $\varepsilon_T f(\frac{t}{t_r})$ is the transient strain, such that $\lim_{t\to\infty} f(t/t_r) = 0$, with t_r the relaxation timescale and ε_T a reference strain.

[7] Transient visco-elastic behaviors as the one described in equations (1) can be mimicked by mechanical analogues based on series of springs and dash-pots (*Joseph* [1990] and Table 1). Two reference cells are classically defined: the

Table 1. Mechanical Analogues of a Viscoelastic Material[a]

Viscoelastic Body	Rheological Equation	Strain Under Constant Stress
Maxwell	$\sigma + \frac{\mu_s}{G_s}\dot{\sigma} = \mu_s\dot{\epsilon}$	$\epsilon = \frac{\sigma_0}{G_s} + \frac{\sigma_0}{\mu_s}t$
Kelvin-Voigt	$\sigma = G_t\epsilon + \mu_t\dot{\epsilon}$	$\epsilon = \frac{\sigma_0}{G_t}\left[1 - \exp\left(-\frac{G_t}{\mu_t}t\right)\right]$
Jeffreys	$\sigma + (\frac{\mu_t}{G_t} + \frac{\mu_s}{G_s})\dot{\sigma} = \mu_s\dot{\epsilon} + \frac{\mu_s\mu_t}{G_t}\ddot{\epsilon}$	$\epsilon = \frac{\sigma_0}{\mu_{(s)}}t + \frac{\sigma_0}{G_t}\left[1 - \exp\left(-\frac{G_t}{\mu_t}t\right)\right]$
Burgers	$\sigma + (\frac{\mu_t}{G_t} + \frac{\mu_s}{G_s} + \frac{\mu_s}{G_t})\dot{\sigma} + \frac{\mu_s\mu_t}{G_sG_t}\ddot{\sigma} = \mu_s\dot{\epsilon} + \frac{\mu_s\mu_t}{G_t}\ddot{\epsilon}$	$\epsilon = \frac{\sigma_0}{G_s} + \frac{\sigma_0}{\mu_s}t + \frac{\sigma_0}{G_s}\left[1 - \exp\left(-\frac{G_t}{\mu_t}t\right)\right]$

[a]In the rheological equations, σ is the stress and ϵ is the strain; σ_0 is the constant stress applied during creep experiments. The two viscosity coefficients μ_s and μ_t, and the two elastic moduli G_s and G_t, are defined in the spring and dashpot mechanical analogue of the viscoelastic bodies.

Maxwell cell (of viscosity μ_s and elastic modulus G_s), formed by a spring and a dash-pot in series, and the Kelvin-Voigt cell (of viscosity μ_t and elastic modulus G_t), formed by a spring and a dash-pot in parallel. The sum of a Kelvin-Voigt cell and a Maxwell cell defines in turn a so-called Burger's body (Table 1). The transient creep of a Burger's body subject to a constant uniaxial stress σ_0 can be analytically expressed as (see Table 1)

$$\epsilon(t) = \frac{\sigma_0}{G_s} + \frac{\sigma_0}{\mu_s}t + \frac{\sigma_0}{G_t}\left[1 - \exp\left(-\frac{G_t}{\mu_t}t\right)\right]. \tag{2}$$

where G_s and G_t are the steady state and transient elastic moduli, μ_s and μ_t are the steady state and transient viscosity. Comparison of equation (2) with equation (1) yields

$$\epsilon_0 \equiv \sigma_0/G_s, \tag{3}$$

$$\dot{\epsilon}_s \equiv \sigma_0/\mu_s, \tag{4}$$

$$\epsilon_T \equiv \sigma_0/G_t, \tag{5}$$

$$t_r \equiv \mu_t/G_t. \tag{6}$$

These equivalences show how the steady response depends on the parameters of the Maxwell cell and how the transient properties depend on the parameters of the Kelvin-Voigt cell.

[8] A Burgers' model provides a satisfying fit of experimental data (Figure 1) and is often used in geology to illustrate the effects of both strain and stress relaxation. However, more detailed experimental studies [e.g., *Cooper*, 2002] have found some important limitations on the applicability of Burger's model to Earth materials. In particular, the initial transient creep can be somewhat underestimated in a Burger's model. A more satisfying fit to the whole set of experimental data is provided by the so-called Andrade model, in which the creep is written as

$$\epsilon(t) = \frac{\sigma_0}{G_s} + \frac{\sigma_0}{\mu_s}t + \epsilon_T\left(\frac{t}{t_r}\right)^n, \tag{7}$$

with $n \approx -1/2$ [*Cooper*, 2002]. This model, initially empirical, is now understood in terms of chemical processes at grain boundaries [*Gribb and Cooper*, 1998]. It can also be represented by a continuous chain of an infinite number of Kelvin-Voigt cells, each having its own relaxation time [*Cooper*, 2002].

[9] The generalization of the rheological equation of an Andrade viscoelastic material to the compaction process, as a function of the properties of its (infinite number of) Kelvin-Voigt cells, is highly challenging. Alternatively, a Burger's model can be taken as the simplest version of the Andrade model (i.e., with one Kelvin-Voigt cell) and can be used to assess some first-order effects of transient creep on viscous compaction. If these effects are important, a further investigation of a complete Andrade model will be necessary, and justified. The easier deciphering of the Burger's model will furthermore provide some important insights on the more complex behavior of the Andrade model.

3. Physical Framework

3.1. Viscous Two-Phase Flow

[10] In the following, we will use the expression "two-phase" flow to describe the circulation of a fluid (liquid) through a compacting much more viscous matrix (solid). For the modeling of viscous compaction, we consider mass and momentum conservation for the fluid and the matrix. The conservation of energy will have to be added to study reactive flows and mass transfer between the two phases [*Spiegelman et al.*, 2001], which is beyond the scope of this paper. The mass conservation and momentum equations for the fluid and the matrix were derived by *McKenzie* [1984]. If the density of each fluid is a constant, mass conservation requires

$$\frac{\partial\phi}{\partial t} + \nabla\cdot\left(v_f\phi\right) = 0, \tag{8}$$

$$\frac{\partial(1-\phi)}{\partial t} + \nabla\cdot\left[V_s(1-\phi)\right] = 0, \tag{9}$$

where ϕ is the porosity of the mixture, and v_f and V_s are the fluid and matrix velocities, respectively. Under the hypothesis that the fluid is much less viscous than the matrix ($\mu_f \ll \mu_s$), the momentum equations comprise a generalized Darcy's law,

$$v_f - V_s = -\frac{k_\phi}{\mu_f\phi}\nabla P, \tag{10}$$

Table 2. Table of Model Parameters

Parameters	Expressions	Dimensions
Reference porosity	ϕ_0	none
Permeability	$K_0 = \phi_0^n a^2/b$	m^2
Grain size	A	m
Tortuosity coefficients	n, b	none
Steady elastic modulus	G_s	Pa
Transient elastic modulus	G_t	Pa
Matrix steady viscosity	μ_s	Pa s
Matrix transient viscosity	μ_t	Pa s
Viscosity ratio	$\lambda_\mu = \mu_t/\mu_s$	none
Elastic modulus ratio	$\lambda_G = G_t/G_s$	none
Fluid viscosity	μ_f	Pa s
Matrix compaction viscosity	$\zeta = \mu_s/\phi^m$, m = 0 or 1	Pa s
Compaction length	$\delta_c = (\mu_s K_0/\mu_f)^{1/2}$	m
Velocity (Darcy's)	$V_0 = K_0/\mu_f(1 - \phi_0)\Delta\rho g$	m s^{-1}
Reference matrix stress	$\tau_0 = \mu_s V_0/\delta_c$	Pa
Density contrast	$\Delta\rho$	kg m^{-3}
Compaction timescale	$t_0 = \delta_c/V_0$	s
Viscoelastic relaxation time	$t_r = \mu_s/G_t$	s
Deborah number	$De = t_r/t_0$	none

and an equation for the viscous compaction of the matrix,

$$\frac{\mu_f V_s}{k_\phi} + (1-\phi)\Delta\rho g - \nabla\cdot\boldsymbol{\tau}_\mathbf{s} = 0, \tag{11}$$

where P is the fluid pressure in excess to hydrostatic pressure, μ_f is the fluid viscosity, $\Delta\rho$ the density contrast between the two phases, g the acceleration of gravity, $\boldsymbol{\tau}_\mathbf{s}$ the stress acting on the matrix, and k_ϕ is the permeability. In the following, will use the Kozeny-Carman relation $k_\phi = \frac{a^2\phi^n}{b}$, with a the grain size, b a geometrical constant, and $n = 3$ (Table 2). Other values are possible for the exponent n, depending on the nature of the rocks and the characteristics of the porous network. The influence of n on compaction has been studied in detail by *Spiegelman* [1993b].

[11] The definition of the rheology of the matrix boils down to the expression of the stress tensor $\boldsymbol{\tau}_\mathbf{s}$. The initial formulation proposed by *McKenzie* [1984] corresponds to a "purely" viscous matrix,

$$\boldsymbol{\tau}_\mathbf{s} = \mu_s\left[\mathbf{e_s} - \frac{1}{3}\mathrm{tr}(\mathbf{e_s})\mathbf{I}\right] + \xi\mathrm{tr}(\mathbf{e_s})\mathbf{I}, \tag{12}$$

where $\mathbf{e_s} = (\nabla V_s) + (\nabla V_s)^t$ is the strain rate tensor (and tr its trace), $\mathbf{I}$ is the identity tensor, and ξ is the compaction viscosity or bulk viscosity. *Scott and Stevenson* [1984] proposed a general expression of ξ as a function of porosity,

$$\xi = \frac{1}{3}\frac{\mu_s}{\phi^m}, \tag{13}$$

with $m = 0$ or 1. More recently, *Bercovici et al.* [2001] demonstrated on the basis of energetic considerations that $m = 1$ in the limit of small porosities. This result can be obtained also from scaling arguments applied to the stress balance at the interface between the fluid and the matrix.

[12] At the interface between the liquid and the matrix, a pressure drop ΔP is generated (1) by surface tension effects and (2) by the difference of viscosity between the two phases. In the following we consider fully miscible fluids and only viscosity differences play a role. At the interface between a liquid pore and the matrix, the balance of normal stresses writes

$$P_s + \boldsymbol{\tau}_\mathbf{s} = P_f + \boldsymbol{\tau}_\mathbf{f}, \tag{14}$$

where P_s and P_f are the pressure in the matrix and in the liquid, respectively, and $\boldsymbol{\tau}_\mathbf{s}$ and $\boldsymbol{\tau}_\mathbf{f}$ are the normal stress in the matrix and in the liquid, respectively. The pressure drop at the interface ΔP scales then as the difference between the liquid and matrix normal stresses. For purely viscous fluids, the normal stress scales as the velocity gradient at the interface times the fluid viscosity. For a shrinking or expanding pore of radius a, the velocity gradient at the interface scales as $a^{-1}\mathrm{d}a/\mathrm{d}t$, and

$$\tau_{f,s} \propto \mu_{f,s}\frac{1}{a}\frac{\mathrm{d}a}{\mathrm{d}t}. \tag{15}$$

If the matrix is much more viscous than the liquid ($\mu_f \ll \mu_s$), the pressure drop will scale as

$$\Delta P = P_s - P_f \approx -\mu_s\frac{1}{a}\frac{\mathrm{d}a}{\mathrm{d}t}. \tag{16}$$

The size of the pores is related to the local porosity, $\phi \approx a^3$, which yields

$$\Delta P = P_s - P_f \approx -\mu_s\frac{1}{\phi}\frac{\partial\phi}{\partial t}, \tag{17}$$

which is similar to the expression obtained by *Bercovici et al.* [2001]. From mass balance, in the limit of small porosity, one gets

$$\frac{\partial\phi}{\partial t} \approx \nabla\cdot V_s, \tag{18}$$

and thus

$$\Delta P \approx -\mu_s\frac{1}{\phi}\nabla\cdot V_s. \tag{19}$$

This pressure drop is similar to the one that would occur in an equivalent compressible viscous medium with a bulk porosity $\xi \propto \mu_s/\phi$, so the rheological equation (12) now writes

$$\boldsymbol{\tau}_\mathbf{s} = \boldsymbol{\mu}_s\left[\mathbf{e_s} + \left(\frac{1}{\phi} - \frac{1}{3}\right)\mathrm{tr}(\mathbf{e_s})\mathbf{I}\right], \tag{20}$$

which is thus consistent with the formalism of *Scott and Stevenson* [1984]. We follow the same line of reasoning to find an expression for the rheological equation of a visco-elastic porous medium.

3.2. Visco-Elastic Rheology

[13] For a visco-elastic matrix, the time derivative of the stress and strain appear in the rheological equation which, for a general Burger-type incompressible material, writes as

$$\boldsymbol{\tau}_\mathbf{s} + t_{r1}\frac{\partial\boldsymbol{\tau}_\mathbf{s}}{\partial t} + t_{r2}^2\frac{\partial^2\boldsymbol{\tau}_\mathbf{s}}{\partial t^2} = \boldsymbol{\mu}_s\left(\mathbf{e_s} + t_{r3}\frac{\partial\mathbf{e_s}}{\partial t}\right), \tag{21}$$

where t_{ri} (i = 1,2,3) are elastic relaxation times for the strain and the stress [*Joseph*, 1990]. The expression of the relaxation timescales is obtained from the rheological parameters of the Burger's body (Table 1),

$$\boldsymbol{\tau}_\mathbf{s} + \left(\frac{\mu_t}{G_t} + \frac{\mu_s}{G_s} + \frac{\mu_s}{G_t}\right)\frac{\partial \boldsymbol{\tau}_\mathbf{s}}{\partial t} + \frac{\mu_s \mu_t}{G_s G_t}\frac{\partial^2 \boldsymbol{\tau}_\mathbf{s}}{\partial t^2} = \mu_s \mathbf{e}_\mathbf{s} + \frac{\mu_s \mu_t}{G_t}\frac{\partial \mathbf{e}_\mathbf{s}}{\partial t}, \tag{22}$$

with μ_s and μ_t the steady and transient viscosity, respectively, and G_s and G_t the steady and transient elastic moduli, respectively. For a porous viscoelastic material, the viscoelastic behavior will be affected (1) by the intrinsic viscoelastic response of the matrix and (2) by the pressure drop (i.e., stress jump) at the interface between the matrix and the fluid.

[14] We first consider a Kelvin-Voigt model, which corresponds to a viscoelastic relaxation of the strain only,

$$\boldsymbol{\tau}_\mathbf{s} = \boldsymbol{\mu}_s\left(\mathbf{e}_\mathbf{s} + t_{r3}\frac{\partial \mathbf{e}_\mathbf{s}}{\partial t}\right). \tag{23}$$

At the interface between the matrix and the fluid, the pressure drop is given by the stress balance as

$$\boldsymbol{\Delta} P = -\boldsymbol{\tau}_\mathbf{s} + \boldsymbol{\tau}_\mathbf{f}. \tag{24}$$

For a Kelvin-Voigt visco-elastic matrix with a much higher viscosity than the liquid, the pressure drop is

$$\boldsymbol{\Delta} P \approx \boldsymbol{\tau}_s \approx -\boldsymbol{\mu}_s\left(\frac{\partial V_s}{\partial r}\right)_{r=a} - \boldsymbol{\mu}_s t_{r3}\frac{\mathrm{D}}{\mathrm{D}t}\left(\frac{\partial V_s}{\partial r}\right)_{r=a}, \tag{25}$$

where D/Dt is the material derivative. Using as above,

$$\frac{\partial V_s}{\partial r} \approx \frac{1}{a}\frac{\mathrm{d}a}{\mathrm{d}t}, \tag{26}$$

$$a \approx \phi^{1/3}, \tag{27}$$

$$\frac{\mathrm{d}a}{\mathrm{d}t} \approx \nabla \cdot V_s, \tag{28}$$

one gets a first-order expression for the pressure drop at the interface

$$\Delta P \approx -\mu_s \frac{1}{\phi}(\nabla \cdot V_s) - \mu_s t_{r3}\frac{1}{\phi}\frac{\mathrm{d}}{\mathrm{d}t}(\nabla \cdot V_s). \tag{29}$$

The resulting rheological equation for the porous matrix is

$$\begin{aligned}\boldsymbol{\tau}_\mathbf{s} = {} & \boldsymbol{\mu}_s\left\{\mathbf{e}_\mathbf{s} - \frac{1}{3}\mathrm{tr}(\mathbf{e}_\mathbf{s})\mathbf{I} + t_{r3}\frac{\partial}{\partial t}\left[\mathbf{e}_\mathbf{s} - \frac{1}{3}\mathrm{tr}(\mathbf{e}_\mathbf{s})\mathbf{I}\right]\right\} \\ & + \boldsymbol{\mu}_s\left\{\frac{1}{\boldsymbol{\phi}}\mathrm{tr}(\mathbf{e}_\mathbf{s})\mathbf{I} + t_{r3}\frac{1}{\phi}\frac{\partial}{\partial t}(\mathrm{tr}(\mathbf{e}_\mathbf{s})I)\right\},\end{aligned} \tag{30}$$

where we have used tr($\mathbf{e}_\mathbf{s}$) instead of $\nabla \cdot V_s$, and where the second term represents the contribution of the pressure jump at the interface.

[15] For a general Burger-type viscoelastic porous medium the visco-elastic behavior will depend (1) on the rate of change of the stress in the matrix and (2) on the rate of change of the stress jump (or pressure jump) at the interface between the matrix and the fluid. This second effect is described by the trace of the stress tensor, which is not zero in the compacting medium, and related to the trace of the strain rate tensor. On the basis of symmetry arguments between strain and stress, and in order to get a similar behavior of $1/\phi$tr($\boldsymbol{\tau}_\mathbf{s}$) and $1/\phi$tr($\mathbf{e}_\mathbf{s}$) in the limit of zero porosity (i.e., traceless stress and strain rate tensors) we propose the following equation,

$$\begin{aligned}\boldsymbol{\tau}_\mathbf{s} + t_{r1}\frac{\partial}{\partial t}\left[\boldsymbol{\tau}_\mathbf{s} + \left(\frac{1}{\phi} - \frac{1}{3}\right)\mathrm{tr}(\boldsymbol{\tau}_\mathbf{s})\mathbf{I}\right] + t_{r2}^2\frac{\partial^2}{\partial t^2}\left[\boldsymbol{\tau}_\mathbf{s} + \left(\frac{1}{\phi} - \frac{1}{3}\right)\mathrm{tr}(\boldsymbol{\tau}_\mathbf{s})\mathbf{I}\right] \\ = \mu\left\{\mathbf{e}_\mathbf{s} + \left(\frac{1}{\phi} - \frac{1}{3}\right)\mathrm{tr}(\mathbf{e}_\mathbf{s})\mathbf{I} + t_{r3}\frac{\partial}{\partial t}\left[\mathbf{e}_\mathbf{s} + \left(\frac{1}{\phi} - \frac{1}{3}\right)\mathrm{tr}(\mathbf{e}_\mathbf{s})\mathbf{I}\right]\right\}.\end{aligned} \tag{31}$$

In the limit case of zero porosity and traceless stress and strain rate tensors, one recovers the equation of a simple visco-elastic Burger-type material.

[16] In the following, the equation are made dimensionless using the classic scaling adopted by *McKenzie* [1984] and given in Table 2, and simplified in the limit of small porosities, taking $1/3 \ll 1/\phi$. This simplification allows easier numerical solutions and can be relaxed if one wants to study the evolution of the system at larger porosity. We also introduce the ratios of transient over steady rheological parameters:

$$\lambda_\mu = \frac{\mu_t}{\mu_s}, \tag{32}$$

$$\lambda_G = \frac{G_t}{G_s}. \tag{33}$$

In one dimension, the resulting conservation equations take the following form,

$$\frac{\partial \phi}{\partial t} = \frac{\partial V_s(1/\phi_0 - \phi)}{\partial z}, \tag{34}$$

$$v_f = -\frac{(1 - \phi\phi_0)V_s}{\phi\phi_0}, \tag{35}$$

$$\frac{\partial \boldsymbol{\tau}_\mathbf{s}}{\partial z} = \frac{1}{K}V_s + \frac{(1 - \boldsymbol{\phi}\boldsymbol{\phi}_0)}{(1 - \boldsymbol{\phi}_0)}, \tag{36}$$

$$\begin{aligned}(\boldsymbol{\phi}\boldsymbol{\phi}_0)\boldsymbol{\tau}_\mathbf{s} + \left(1 + \lambda_G + \phi\lambda_\mu\right)\mathrm{De}\frac{\partial \boldsymbol{\tau}_s}{\partial t} + \mathrm{De}^2\left(\lambda_G\lambda_\mu\right)\frac{\partial^2 \boldsymbol{\tau}_\mathbf{s}}{\partial t^2} \\ = \frac{\partial V_s}{\partial z} + \mathrm{De}\lambda_\mu\frac{\partial^2 V_s}{\partial z \partial t},\end{aligned} \tag{37}$$

where in the dimensionless rheological equation of the porous medium, a new dimensionless number is introduced, the Deborah number De [*Reiner*, 1964],

$$\mathrm{De} = \frac{\mu_s}{\lambda_G G_s t_0} = \frac{\mu_s}{G_t t_0}. \tag{38}$$

This number is defined as the ratio of two timescales, an elastic relaxation timescale $t_r \equiv \mu_s/G_t$, and the compaction timescale t_0 (Table 2). To further simplify the equations, as λ_G and λ_μ are smaller than 1, because the transient parameters are smaller than the steady ones [*Chopra*, 1997], we will also assume $1 + \lambda_G + \phi\lambda_\mu \approx 1$.

[17] Some reference studies of viscous compaction were performed without taking into account the pressure drop at the interface between the matrix and the liquid. In that case, which is not physically consistent (see the detailed discussion by *Bercovici et al.* [2001]), $m = 0$ in equation (13) and the rheological equation writes as

$$\boldsymbol{\tau_s} + \mathrm{De}\frac{\partial \boldsymbol{\tau_s}}{\partial t} + \mathrm{De}^2\left(\boldsymbol{\lambda_G}\boldsymbol{\lambda_\mu}\right)\frac{\partial^2 \boldsymbol{\tau_s}}{\partial t^2} = \frac{\partial V_s}{\partial z} + \mathrm{De}\boldsymbol{\lambda_\mu}\frac{\partial^2 V_s}{\partial z \partial t}. \tag{39}$$

For the sake of the comparison with these previous reference studies, we will use the general form

$$(\phi\phi_0)^m \boldsymbol{\tau_s} + \mathrm{De}\frac{\partial \boldsymbol{\tau_s}}{\partial t} + \mathrm{De}^2\left(\boldsymbol{\lambda_G}\boldsymbol{\lambda_\mu}\right)\frac{\partial^2 \boldsymbol{\tau_s}}{\partial t^2} = \frac{\partial V_s}{\partial z} + \mathrm{De}\boldsymbol{\lambda_\mu}\frac{\partial^2 V_s}{\partial z \partial t}, \tag{40}$$

with $m = 0$ or 1.

[18] The model we propose for a Burger's porous medium includes as limit cases the rheologies previously studied in the literature. For De = 0, the model corresponds to the classic purely viscous compaction. For De $\neq$ 0, $\lambda_G = 1$ and $\lambda_\mu = 0$, our formalism is equivalent to the Maxwell rheology used by *Connolly and Podladchikov* [1998]. One should note, however, that in the work of *Connolly and Podladchikov* [1998], visco-elasticity is related to compressibility, whereas here the fluids are incompressible and visco-elasticity corresponds to transient creep of the matrix (with a specific contribution of the pressure jump at the interface between the liquid and the matrix). In the full Burger's formalism (arbitrary λ_G), the Deborah number is a function of the transient elastic modulus G_t and not a function of the steady elastic modulus G_s as in a Maxwell body (equation (38)). As the transient elastic modulus G_t is smaller than the steady one G_s, the Deborah number, and thus the associated elastic effects, are going to be larger in transient creep than for a Maxwell body. In the next section we illustrate in details the implications of the transient creep as a function of the Deborah number De, and of the viscosity and elastic modulus ratios, λ_μ and λ_G.

4. Numerical Modeling of Visco-Elastic Compaction

[19] We perform 1-D numerical simulations in order to quantitatively investigate the effects of the dimensionless parameters of the rheological equation (39). The system of dimensionless equations (34) to (36) and equation (39) is numerically solved to calculate the evolution of a finite Gaussian porosity disturbance

$$\phi = 0.2 + 0.8\exp\left[-(z-10)^2\right]. \tag{41}$$

Note here that as ϕ is dimensionless, the small porosity assumption is insured by the value of the porosity-scale $\phi_0 = 0.04$. A dimensionless porosity of 1 corresponds thus to a 4% liquid fraction. We used a finite difference method with a second-order scheme in time as in the work of *Barcilon and Richter* [1986], and an iterative method for the coupled variables $\boldsymbol{\tau_s}$ and V_s.

4.1. Reference Calculation

[20] We first performed a set of reference calculations in the purely viscous regime (De = 0), and in a regime with dominant elastic effects and no transient creep (De = 0.5, $\lambda_\mu = 0$), for $m = 0$ and $m = 1$. The classical viscous solution is illustrated Figure 2a for $m = 0$ and Figure 2b for $m = 1$. For the two cases, solitons are generated and propagate with constant velocity while maintaining a constant shape. For $m = 1$ the amplitude and the velocity are smaller than for $m = 0$. A more detailed discussion of the effects of m is given by *Rabinowicz et al.* [2002] for a step-like porosity disturbance.

[21] The elastic solution (De = 0.5) is drawn Figure 2e for $m = 0$ and Figure 2f for $m = 1$. A similar shock wave is generated in the two cases, as already observed by *Connolly and Podladchikov* [1998]. The shock wave stays attached to its source region and spreads as it propagates. The velocity of the propagation front thus decreases as a function of time. For values of De between 10^{-2} and 10^{-1}, the solution is intermediate between the two previous end-members, as illustrated Figures 2c and 2d for De = 5 10^{-2}. A complete discussion of these cases can be found in the work of *Vassilyev et al.* [1998].

4.2. Limit of Small Transient Elastic Modulus, $\lambda_G \rightarrow 0$

[22] We have already mentioned that a Maxwell body is a limit case of the Burger's formalism for small transient viscosities ($\lambda_\mu \rightarrow 0$). Another limit case, the Jeffrey's body, is defined for small transient elastic moduli ($\lambda_G \rightarrow 0$). A Jeffrey's body corresponds to the simplest model of a transient creep that evolves toward a steady viscous regime [*Joseph*, 1990]. As shown by the expression of the right member of equation (39), the viscosity ratio λ_μ controls the strain relaxation. For too small values of De there are no elastic effects and the Jeffrey's model behaves purely viscously. We thus focus on the calculation results obtained for intermediate and large De.

[23] Figure 3 shows the propagation of the porosity disturbance through a Jeffrey's porous medium with $m = 0$, for different values of De and λ_μ. For intermediate De ($10^{-2} < \mathrm{De} < 10^{-1}$), and small λ_μ ($\approx 10^{-1}$), the propagation occurs in an elastic mode and there is no influence of λ_μ (Figures 2c and 3a). For $\lambda_\mu \approx 1$ (Figures 3b and 3d), the propagation is equivalent to that in a purely viscous medium, and solitary waves are generated for all De. This result can be understood by noting that the viscous stress $\boldsymbol{\tau_s} = \frac{\partial V_s}{\partial z}$

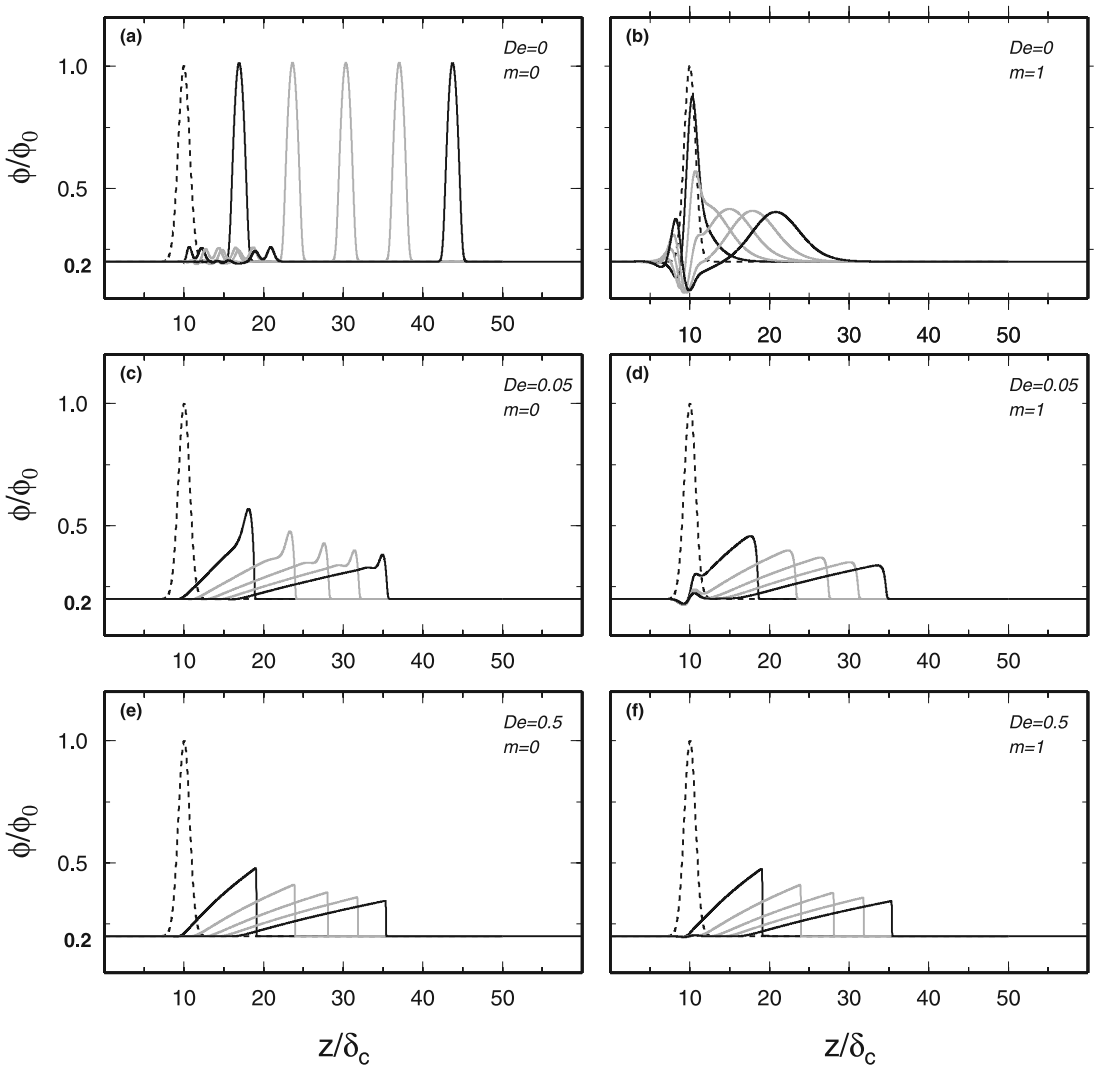

Figure 2. Evolution of dimensionless porosity as a function of dimensionless distance for an initial Gaussian distribution, for three different Deborah numbers and with (m = 1) or without (m = 0) porosity dependence of the compaction viscosity. For each figure, porosity is shown at t = 0 (dashed line), t = 0.6 (solid black line), t = 1.2, 1.8 and 2.4 (solid gray line), and t = 3 (solid black line.) Elastic propagation occurs in an elastic mode (shock waves) for De = 0.05 and De = 0.5, whereas the viscous mode (solitary waves) is obtained for De = 0.

(independent of De) is a solution of the Jeffrey's rheological equation for m = 0,

$$\tau_s + \mathrm{De}\frac{\partial \tau_s}{\partial t} = \frac{\partial V_s}{\partial z} + \mathrm{De}\frac{\partial}{\partial t}\left(\frac{\partial V_s}{\partial z}\right). \tag{42}$$

[24] The case for large De (De > 0.1) and small λ_μ ($\approx 10^{-1}$) is more complex (Figure 3c): the propagation first starts like in a viscous mode and individual peaks appear. These peaks are sharper than in the reference viscous case, as their length scale is controlled by the transient viscosity which is smaller than the steady one (λ_μ < 1). The amplitude of the peaks decreases along the propagation by mass conservation, because the elastic response of the medium (large De) does not allow the background porosity to go back to its initial value behind the peaks. This effect has been also described in the case of a Maxwell body by *Connolly and Podladchikov* [1998]. The long-term evolution of the peaks is thus to disappear and the propagation will evolve toward a shock wave as in the Maxwell case.

[25] Figure 4 shows the same calculations as in Figure 3 but for m = 1. For small viscosity ratios, $\lambda_\mu \approx 0.1$, the results are close to the ones found for m = 0 (Figures 3a, 3c, 4a, and 4c). The porosity dependence of viscosity (m = 1) has, however, a large effect for λ_μ = 1: the viscous stress is not a solution of the rheological equation anymore and shock waves are generated instead of solitary waves. For De = 0.05 (Figure 4b) a peak appears at the propagation front, but its velocity is not large enough (because of the compaction viscosity) to allow its detachment to form a solitary wave. For De = 0.5 (Figure 4d), the elastic response of the matrix balances the effect of the compaction viscosity at the front

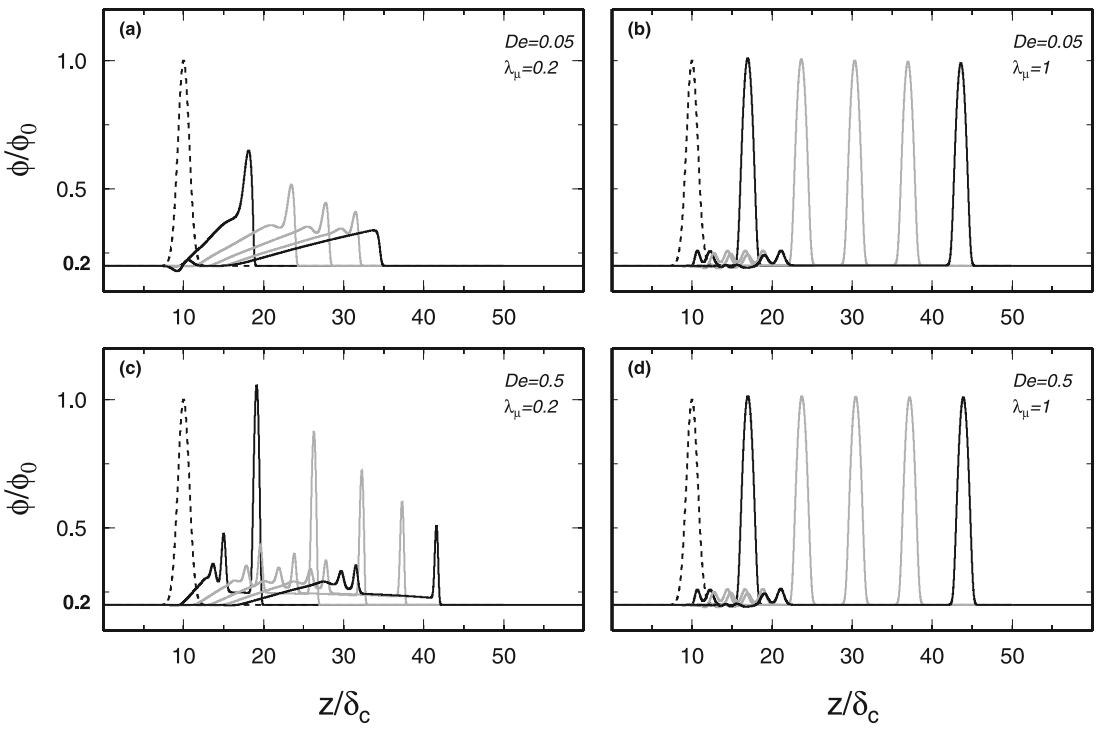

Figure 3. Evolution of porosity for a Jeffreys body ($\lambda_G = 0$) with $m = 0$ and for different values of De and viscosity ratio λ_μ. The curves are shown for the same times as in Figure 1. For any De, $\lambda_\mu = 1$ produces a viscous compaction.

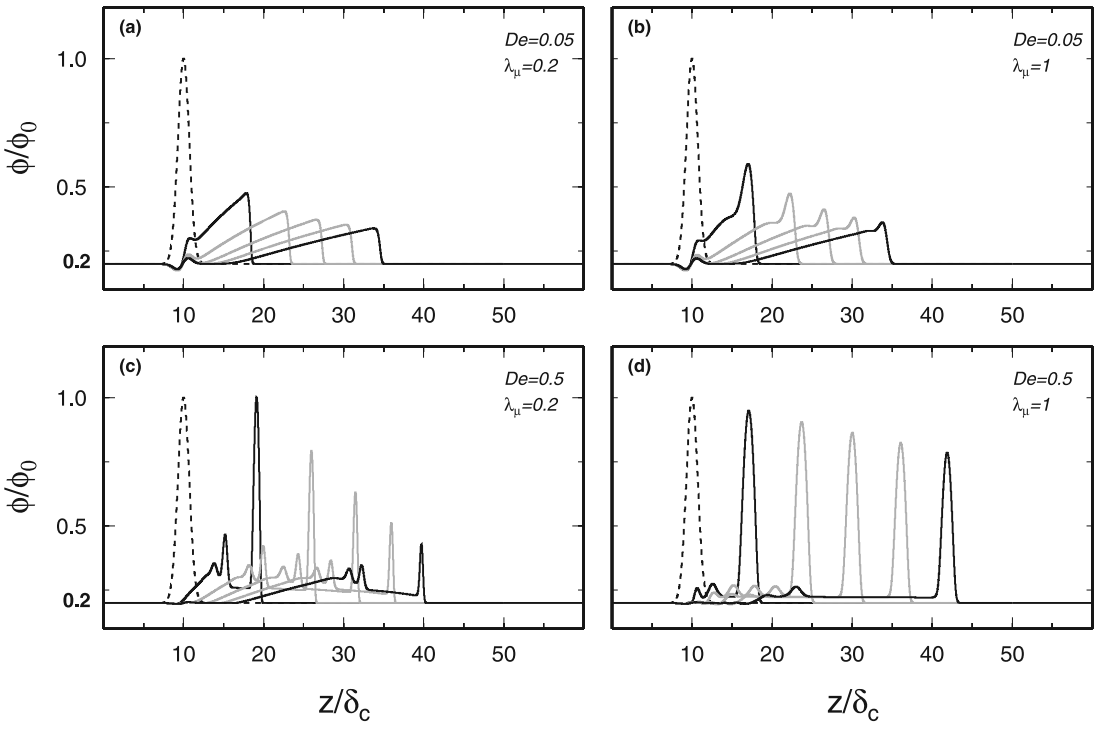

Figure 4. Evolution of porosity for a Jeffreys body with $m = 1$ and for different values of De and viscosity ratio λ_μ. The curves are shown for the same times as in Figure 1. For large De (De = 0.5) and $\lambda_\mu = 1$ "quasi" solitary waves are generated.

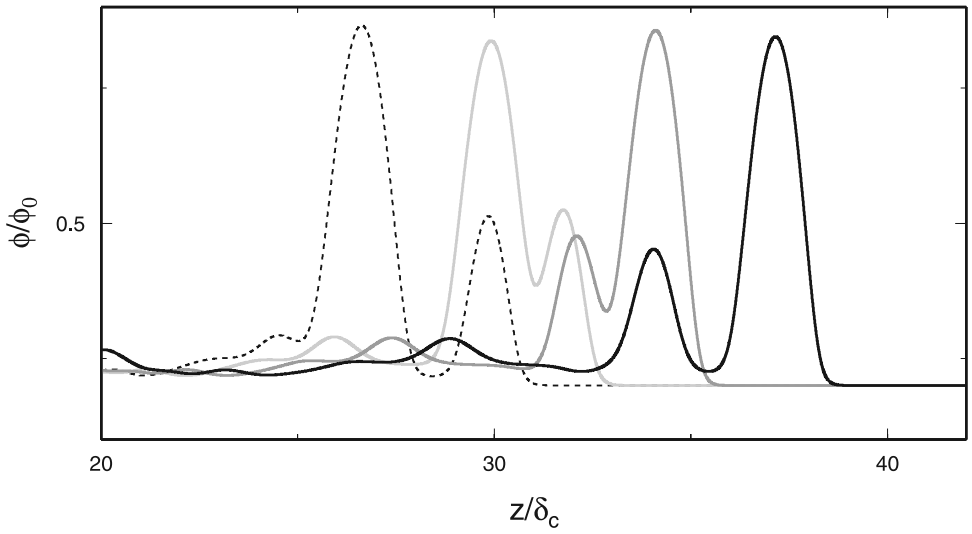

Figure 5. Interaction between two "quasi" solitary waves for a Jeffrey's body with $m = 1$, De = 0.5 and $\lambda_\mu = 1$. The curves are shown at $t = 1.2$ (dashed line), $t = 1.44$ (light gray line), $t = 1.68$ (gray line) and $t = 1.92$ (black line). The two waves keep a same shape after and before their interaction, like solitary waves. There is, however, a small damping of their amplitude along their propagation.

of the peak and favors its detachment. In the limit of very large De (and $\lambda_\mu = 1$), the rheological equation will write as

$$\mathrm{De}\frac{\partial \boldsymbol{\tau}_\mathbf{s}}{\partial t} = \mathrm{De}\frac{\partial^2 V_s}{\partial z \partial t}, \tag{43}$$

of which the purely viscous stress $\boldsymbol{\tau}_\mathbf{s} = \partial V_s/\partial z$ is a solution. Solitary waves will thus form at large De in a Jeffrey's body, whereas in the case of a Maxwell body a large De favors the formation of shock waves. The amplitude of the waves, however, decreases along their propagation; in the present case (De = 0.5), it is reduced by a factor 2 when the wave has traveled over 180 compaction lengths (defined in Table 2). This is again due to the fact that elasticity prevents the background porosity from going back to its initial value at the back of the peak. To illustrate further the "quasi" solitary waves behavior of the peak, we computed the interaction between two waves generated by the following initial porosity profile:

$$\phi = 0.2 + 0.8\exp\left[-(z-10)^2\right] + 0.4\exp\left[-(z-20)^2\right], \tag{44}$$

with $De = 0.5$ and $\lambda = 1$. The result displayed in Figure 5 shows indeed that the "quasi solitary waves" conserve their shape after their interaction.

4.3. Full Burger's Model

[26] The interpretation of the behavior of a porous Burger's body is not as straightforward as the cases of a Maxwell body or a Jeffrey's body. As a matter of fact, the term associated with the second time derivative of the stress in the rheological equation (39) introduces a coupling between the three rheological parameters (De, λ_μ, λ_G). We propose in the following a systematic comparison between the results obtained for a Jeffrey's model to the ones obtained for a full Burger's model in order better to understand the implications of this coupling. We have obtained during some preliminary calculations that the porosity dependence had only a secondary effect and we will thus focus here on the case $m = 1$.

[27] Figure 6 shows the propagation of the porosity disturbance for the full Burger's model at intermediate De ($\mathrm{De} = 5.10^{-2}$). The comparison of Figure 6 with Figures 4a and 4b illustrates the effect of λ_G. Small-scale additional peaks appear at the propagation front. Their length scale is a decreasing function of λ_G and λ_μ, whereas their number is an increasing function of λ_G. The propagation of the wave as a whole is, however, not much different than that of the reference shock wave. In the following we will refer to this propagation mode as "shaggy" shock waves.

[28] The effect of λ_G at large De is illustrated Figure 7. The comparison between Figures 7a, 7b, and 4c shows that for a small viscosity ratio ($\lambda_\mu \approx 0.1$) extra peaks still appear at the propagation front. Their length scale is a decreasing function of λ_G whereas the number of peaks is an increasing function of λ_G. For a viscosity ratio λ_μ of order unity, there is a detachment of the peaks to form a wave train (Figures 7c and 7d). These peaks can be compared to the ones obtained for a Jeffrey's body (Figure 4d). The length scale of the Burger's peaks is much reduced, and their amplitude is much larger than for a Jeffrey's body, as a function of λ_G. The velocity of the Burger's peaks is also much larger. There is, however, a similar damping in the Burger case as in the Jeffrey case, due to the elastic relaxation of the background porosity at the back of the peak. We have checked that the Burger's peaks behave as the Jeffrey's peaks like "quasi" solitary waves. We will refer to that compaction regime as "polytons" in the following.

[29] As a conclusion, we have obtained two families of propagation modes in the full Burger's model. The first family, obtained for small De ($\mathrm{De} < 10^{-2}$) corresponds to the classic viscous solitary waves. The second family, obtained for larger De ($\mathrm{De} > 10^{-2}$) corresponds to a visco-elastic propagation. As a function of the viscosity ratio λ_μ and of the elastic modulus ratio λ_G, three propa-

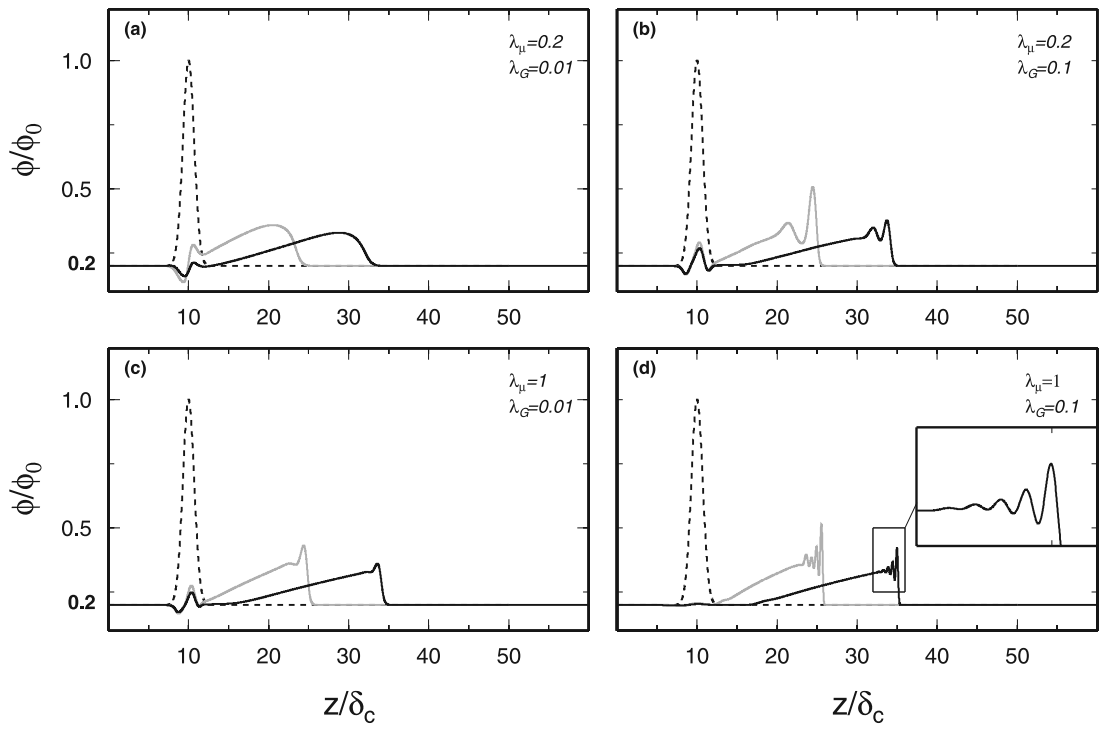

Figure 6. Evolution of porosity for a full Burger's body with $m = 1$ and an intermediate Deborah number De = 0.05, and for different values of viscosity ratio λ_μ and elastic modulus ratio λ_G. The curves are shown at $t = 0$ (dashed line), $t = 1.5$ (thin gray line), and $t = 3$ (black line). The reference shock wave predicted for a Maxwell body evolves into a "shaggy" shock wave presenting additional small-scale peaks at the propagation front.

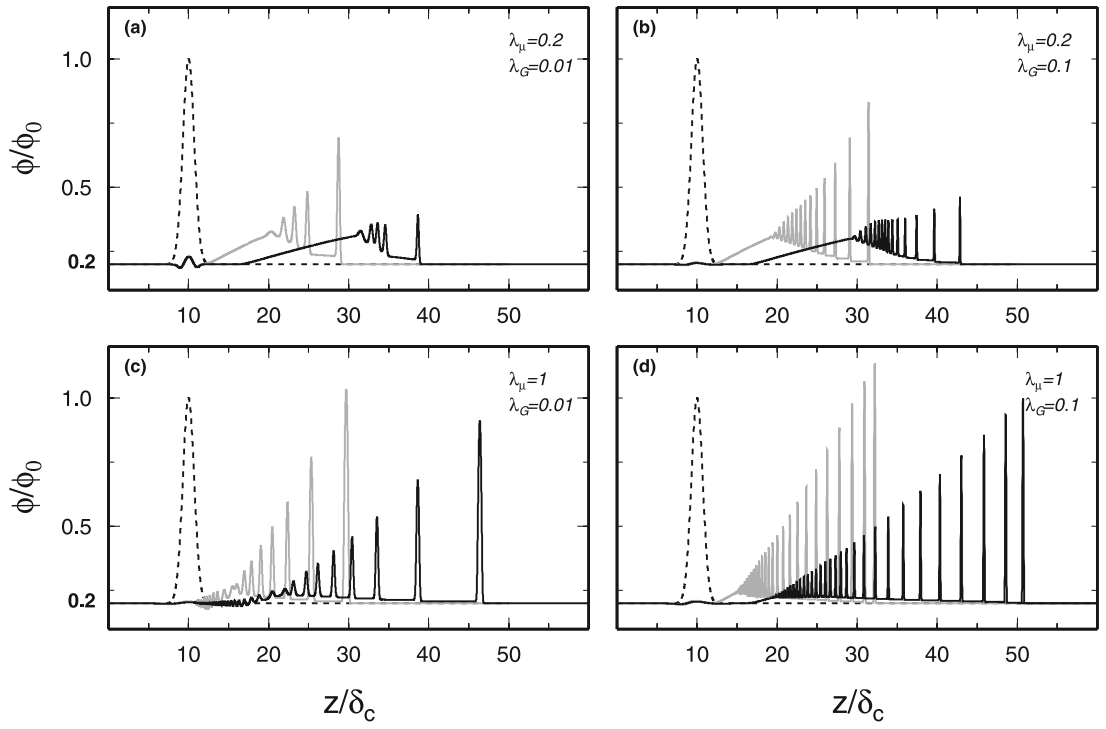

Figure 7. Evolution of porosity for a full Burger's body with $m = 1$ and a large Deborah number De = 0.5, and for different values of viscosity ratio λ_μ and elastic modulus ratio λ_G. The curves are shown at $t = 0$ (dashed line), $t = 1.5$ (thin gray line), and $t = 3$ (black line). The reference shock wave predicted for a Maxwell body evolves into a train of peaks of small length scale and large amplitude, or "polytons".

Table 3. Rheological Parameters for Earth Materials

Material	λ_G	λ_μ	Reference	Method
Olivine rocks	0.05–0.36	0.17–0.65	*Chopra* [1997]	creep experiments
Dunite Mr. Burnet	0.03	0.15	*Post* [1977]	creep experiments
Wet Olivine	0.019–0.474	0.211–0.79	*Mackwell et al.* [1985]	creep experiments
Upper mantle	1	0.35	*Pollitz* [2003]	postseismic deformation
Argillite	0.1–1	0.01–0.1	*Gunzburger and Cornet* [2007]	creep experiments
Lower crust	1	0.004	*Pollitz* [2003]	postseismic deformation

gation modes have been identified: shock waves, "shaggy" shock waves, and a train of "quasi" solitary waves or "polytons". The precise characterization of the two new propagation modes we have identified in the Burger's model (shaggy shock waves and polytons) will require a more detailed mathematical study and is beyond the scope of this paper. In the next section we restrict ourselves to the discussion of first-order implications of the Burger's model for the propagation of fluids in the Earth as a function of the expected values of the rheological parameters (De, λ_μ and λ_G.)

5. Discussion

[30] We have shown in the previous section that the propagation of a porosity disturbance through a Burger's porous medium is a function of the Deborah number (De), the viscosity ratio (λ_μ) and the ratio of elastic moduli (λ_G). We first discuss the values expected for these parameters in the Earth, and then investigate the implications for the circulation of melt, petroleum and CO_2. To keep things simple, we consider that the compaction viscosity is a function of the porosity, $\zeta \propto \mu_s/\phi$, which corresponds to $m = 1$.

5.1. Values of the Rheological Parameters λ_μ, λ_G and De for Geological Materials

[31] Transient rheology of Earth materials can be studied at different scales, from laboratory experiments to geological measurements, such as stress profiles in boreholes [*Gunzburger and Cornet*, 2007], postseismic deformations [*Pollitz*, 2003] or postglacial rebound [*Yuen and Sabadini*, 1986]. The inferred values of the ratios of viscosities and elastic moduli are given in Table 3. One may note that λ_μ is always strictly smaller than 1 whereas λ_G is always larger than 0. This implies that a full Burger's formalism is indeed required (and maybe a more complex Andrade model) to study the compaction of geological materials. The resulting compaction regime is a function of the Deborah number.

[32] The Deborah number is defined in equation (38). In this equation, De is a function of the transient elastic modulus G_t rather than of the steady elastic modulus G_s. As $\lambda_G = G_t/G_s \leq 1$, the effective value of the Deborah number in the full Burger's model is larger than the estimations provided in the literature for Maxwell models in which De is a function of G_s [e.g., *Connolly and Podladchikov*, 1998].

[33] For melt extraction in the mantle, we take $G_s = 10^{11}$ Pa, $\mu_s = 10^{21}$ Pa s, $\mu_f = 1$ Pa s, $\Delta\rho = 500$ kg m^{-3}, $b = 250$, n

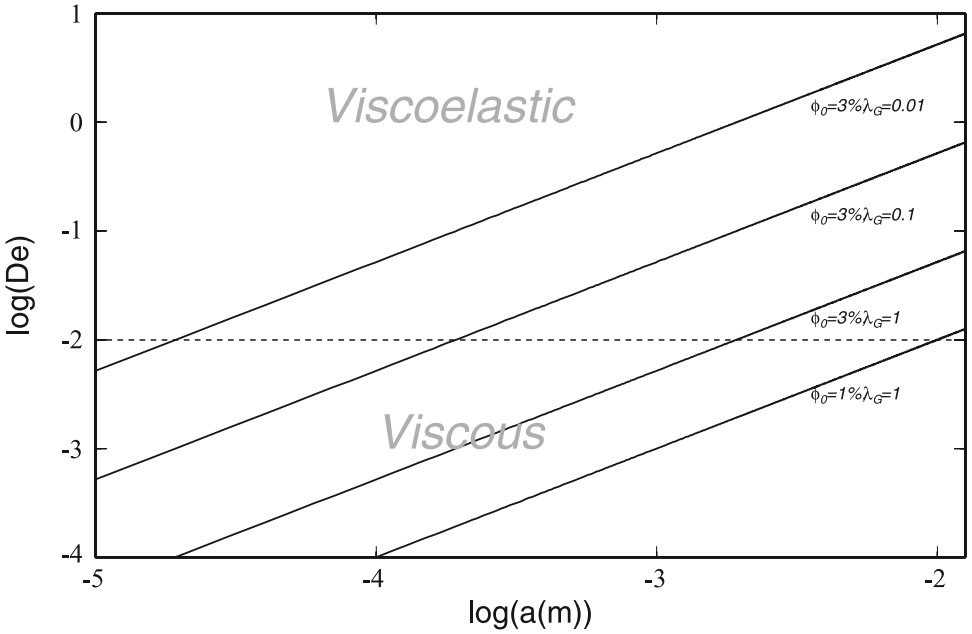

Figure 8. Effective Deborah number in the mantle as a function of the grain size, for a decreasing ratio of elastic moduli λ_G and for a background porosity ϕ_0 of 1% and 3%. The transition between viscous and elastic compaction occurs for De = 0.01. A large grain size, a large background porosity, as well as a small elastic modulus ratio λ_G favor visco-elastic compaction.

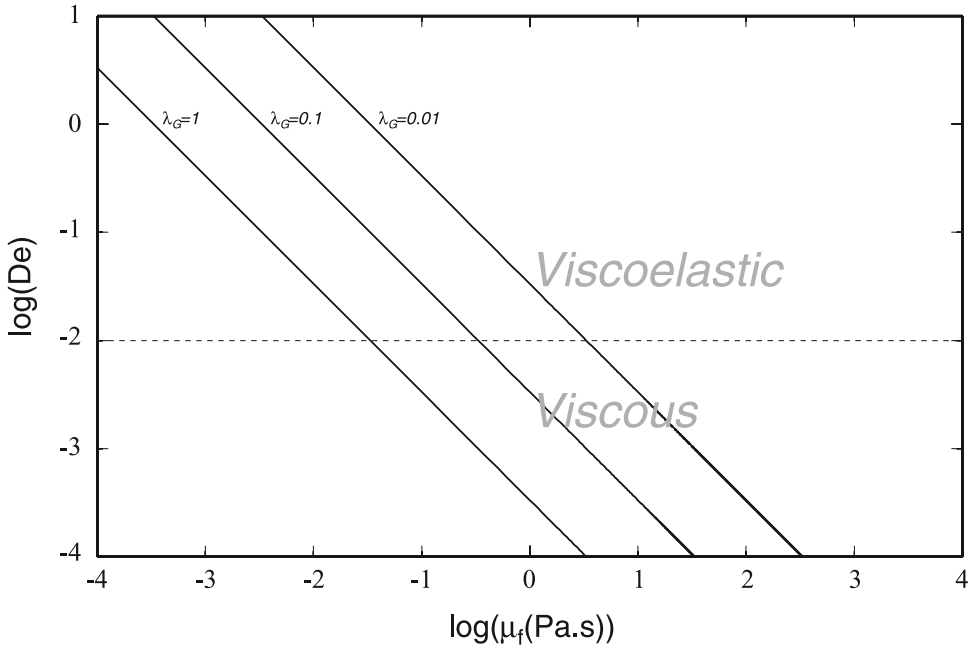

Figure 9. Effective Deborah number in sedimentary basins as a function of the viscosity of the fluid phase, for a decreasing ratio of elastic moduli λ_G and for a background porosity ϕ_0 of 3%. The transition between viscous and elastic compaction occurs for De = 0.01. A small fluid viscosity as well as a small elastic modulus ratio λ_G favor visco-elastic compaction.

= 3, and we estimate De as a function of the grain size a for different values of λ_G and ϕ_0. The result presented in Figure 8 allows one to define a minimum grain size for which the visco-elastic threshold (De $\geq 10^{-2}$) is reached as a function of λ_G and ϕ_0. A minimum estimate is obtained for $\phi_0 = 0.03$ and $\lambda_G = 0.01$, which yields $a \geq 0.05$ mm. A maximum estimate is obtained for $\phi_0 = 0.01$ and $\lambda_G = 1$, which yields $a \geq 10$ mm. Grain size in the mantle can be obtained by the study of seismic attenuation in polycrystalline olivine, which is also due to the visco-elastic behavior of the grains. By an extrapolation of laboratory measurements, *Jackson et al.* [2002] showed that a grain size of few millimeters is required by seismic attenuation in the mantle. We can thus conclude that for a realistic value of the reference porosity and for the values of λ_G expected in the mantle (Table 3), visco-elastic effects have to be taken into account in the modeling of mantle compaction.

[34] Sedimentary basins are the second geological environment in which visco-elastic compaction is likely to play a role, both for the migration of water during diagenesis and for the migration of petroleum [e.g., *Suetnova and Vasseur 2000*]. For compaction in sedimentary basins, we take $G_s = 10^{11}$ Pa, $\mu_s = 10^{21}$ Pa s, $\Delta\rho = 1500$ kg m^{-3}, $a = 1$ mm, $\phi = 0.03$, $b = 250$, $n = 3$, and we estimate De as a function of μ_f for different values of λ_G. The chosen value for G_s is an upper bound and yields a lower bound for the Deborah number and visco-elastic effects. We choose here to use μ_f as a free parameter, as compaction in a sedimentary basins is going to be a function of the nature and viscosity of the fluid expelled: water, light petroleum, or liquid CO_2 ($\mu_f \approx 10^{-3}$ Pa s), or heavy petroleum ($\mu_f \approx 10^3$ Pa s). The result presented in Figure 9 shows that a fluid with a viscosity larger than 10 Pa s (heavy petroleum) will always propagate in the viscous mode. On the other hand a fluid with a viscosity smaller than 0.1 Pa s (light petroleum, CO_2) will always propagate in a visco-elastic mode. The propagation mode of fluids with an intermediate viscosity will depend on λ_G. Visco-elastic effects have thus to be taken into account at least to quantitatively model low-viscosity fluids migration at depth in sedimentary basins.

5.2. Regime Diagrams for Visco-Elastic Compaction in the Earth

[35] For small values of De (De $\leq 10^{-2}$), compaction is purely viscous. Visco-elastic compaction will occur for larger De, and we present here two regime diagrams that define the visco-elastic extraction mode for intermediate and large values of De, as a function of the expected viscosity and elastic modulus ratios (λ_μ and λ_G, respectively) for Earth materials.

[36] Figure 10 shows the regime diagram for large De (De = 0.5). Three extraction modes are possible, shock waves, shaggy shock waves, and polytons. The viscosity ratio λ_μ is the main parameter to define the boundaries between the three regimes. The transition from shock waves to shaggy shock waves occurs for $\lambda_\mu > 10^{-2}$, whereas polytons are generated for $\lambda_\mu > 10^{-1}$. The threshold values of λ_μ are a weak decreasing function of λ_G. If De is large, polytons are the most likely mode of compaction in the mantle whereas shaggy shock waves are more likely in sedimentary basins. At even larger Deborah numbers, that may be relevant for sedimentary basins, polytons are also expected.

[37] Figure 11 presents the regime diagram for intermediate De (De = 5 10^{-2}). Only two extraction modes are possible, shock waves and shaggy shock waves. For λ_G larger than 0.1 the boundary between the two regimes is given by $\lambda_\mu > 0.1$. For λ_G smaller than about 0.05, only shock waves occur. For intermediate values of De, com-

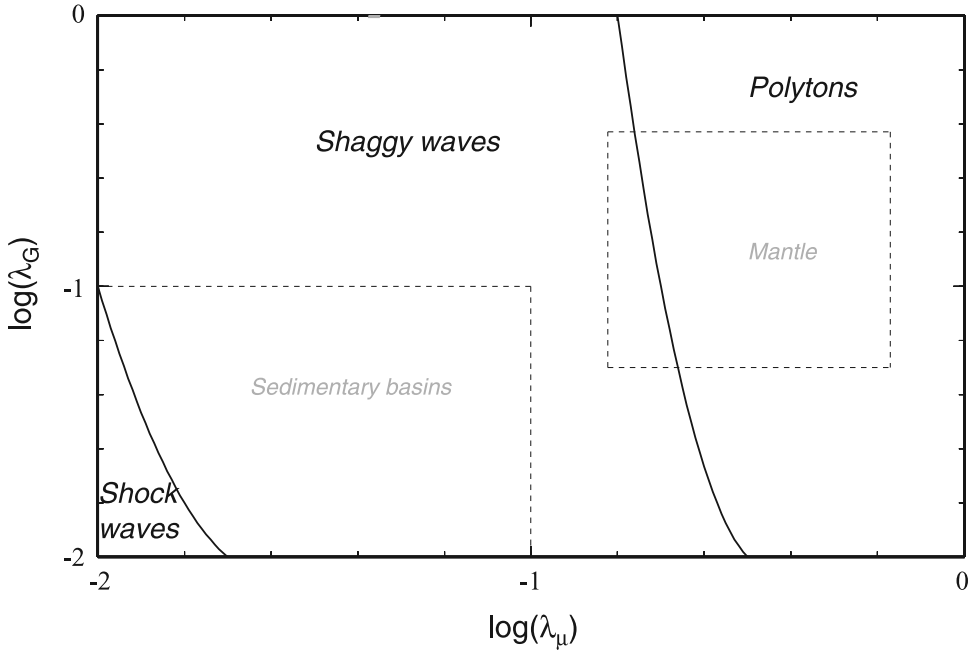

Figure 10. Compaction regime diagram for Earth materials at large De (De = 0.5) as a function of viscosity ratio λ_μ and elastic modulus ratio λ_G. Three propagation modes can occur for an increasing λ_μ: shock waves, shaggy shock waves and polytons. Typical range of parameters are shown for the mantle [*Chopra*, 1997] and sedimentary basins [*Gunzburger and Cornet*, 2007]. Polytons are expected in the mantle whereas shaggy shock waves are expected in sedimentary basins.

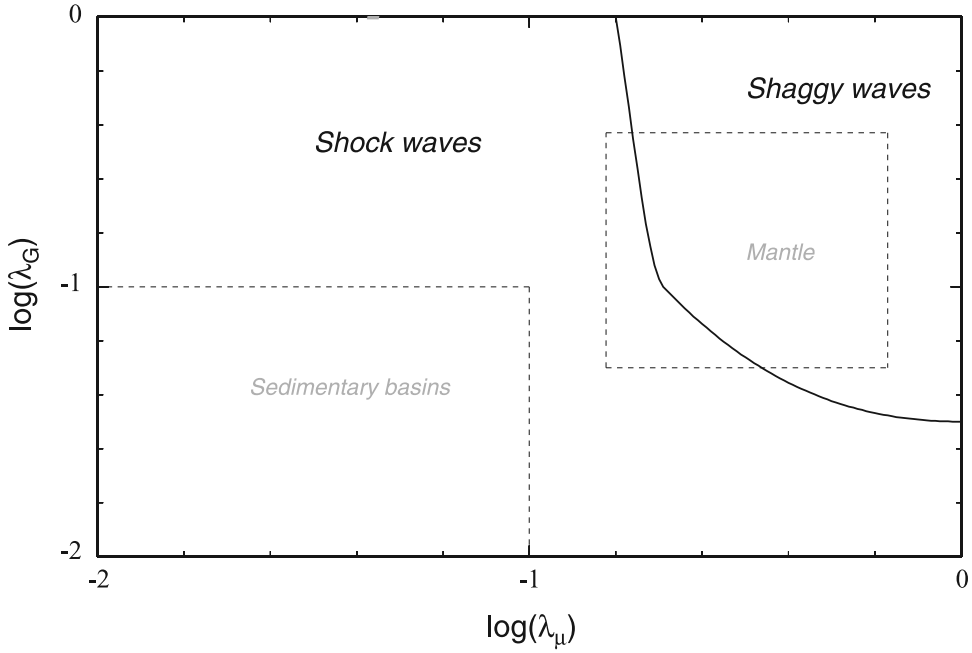

Figure 11. Compaction regime diagram for Earth materials at intermediate De (De = 0.05) as a function of viscosity ratio λ_μ and elastic modulus ratio λ_G. Only two propagation modes can occur for an increasing λ_μ: shock waves and shaggy shock waves. Typical range of parameters are shown for the mantle [*Chopra*, 1997] and sedimentary basins [*Gunzburger and Cornet*, 2007]. For an intermediate Deborah number, shaggy shock waves are expected in the mantle whereas regular shock waves are expected in sedimentary basins.

paction will always occur in the shock wave regime in sedimentary basins, whereas mantle compaction will occur in the shaggy shock wave regime for large values of λ_G. Polytons are not expected in the mantle or in sedimentary basins for intermediate De.

5.3. Geological Perspective

[38] In the eighties, the development of the theoretical concept of solitary waves associated with viscous compaction [*Richter and McKenzie*, 1984; *Barcilon and Richter*, 1986] has changed the view of geodynamicists on melt propagation in the mantle and the interpretation of geochemical characteristics of lava. The signature of many subsurface geological processes can be associated with characteristics of porous solitary waves too [e.g., *Revil*, 2002b; *Revil and Cathles*, 2002; *Miller et al.*, 2004; *Fontaine et al.*, 2003]. Such waves are not predicted by classic Maxwell models that only produce shock waves at the large Deborah numbers expected in these geological environments. Viscous compaction has been advocated to explain porosity waves in sedimentary basins [*Fowler and Yang*, 1999; *Brown*, 2000]. However, purely viscous compaction requires quite restrictive conditions to allow efficient fluid extraction in sedimentary basins [*Appold and Nunn*, 2002]. It is furthermore not the dominant deformation mechanism at the high Deborah numbers expected in sedimentary basins. Our complete visco-elastic model, which incorporates both stress and strain relaxation, can generate a train of quasi solitary waves (polytons) that mimic the characteristics of viscous waves at large Deborah number. It thus provides a new framework to better constrain and interpret the transport of hydrocarbon. They are also an important mechanism to consider when testing long-term geological confinement of CO_2. However, some limitations of our model will have to be relaxed first in order to allow its full quantitative use.

[39] First, the results presented here have been established by solving a set of 1-D equations. One-dimensional porosity waves are intrinsically unstable and will evolve toward 2-D and then 3-D waves [*Barcilon and Richter*, 1986]. The characteristics of such 3-D waves are not fully known for a purely viscous material but they are supposed to form a large-scale network of high-porosity channels, as a function of complex interactions between compaction, chemical reactions and/or shear deformation of the medium [*Wiggins and Spiegelman*, 1995; *Spiegelman and Kelemen*, 2003; *Spiegelman*, 2003]. Such a complexity will have to be included too in a full 3-D visco-elastic model. Second, we have considered here constant rheological parameters only. However, both viscosity and elastic moduli are likely to depend on porosity. The interplay between viscosity and porosity bears some important implications for the evolution of the porosity waves, such as described by *Khodakovskii et al.* [1995]. The transient elasticity increases with the melt fraction [*Green and Cooper*, 1993] which will help the transition from shaggy waves (intermediate λ_G) to polytons (large λ_G). Such effects are important and will require a specific study. Third, as already stated in the introduction, a Burgers' model is a much simplified representation of the more complex visco-elastic behavior of geological materials. These materials are likely to be characterized by a distribution of elastic relaxation timescales, as a function of the distribution of grain sizes for example [*Revil et al.*, 2006]. Andrade's models display a distribution of elastic relaxation timescales and reproduce the behavior of geological materials [*Cooper*, 2002]. However, the generalization of an Andrade model to a porous medium remains very challenging. The results obtained here for a Burger's model provide a strong motivation to try to adapt the Andrade's formalism to porous medium. They will prove very useful in the deciphering of the complex behavior of the Andrade's model. For example, one may note that Andrade's models correspond to smaller transient viscosity than Burger's models [*Cooper*, 2002], which will tend to somewhat impend the generation of polytons. The generalization of our formalism to an Andrade model will be the scope of a next study.

6. Conclusion

[40] The effect of transient creep on the compaction process in the Earth has been incorporated to a two-phase flow theory on the basis of a Burger's model. The rheology of the porous material is a function of three dimensionless numbers: (1) the Deborah number, defined by the ratio of an elastic relaxation timescale over the compaction timescale, (2) the ratio of the transient viscosity over the steady viscosity, and (3) the ratio of the transient elastic modulus over the transient elastic modulus. For a Deborah number larger than 10^{-2}, visco-elastic effects become important. Visco-elastic compaction can occur in three different regimes, as a function of the rheological parameters, shock waves, shaggy shock waves and polytons. The two last regimes are characteristic of transient creep.

[41] Large Deborah numbers are expected in sedimentary basins and in the upper mantle. Visco-elastic effects during compaction cannot be neglected in general. In the mantle, for large Deborah numbers corresponding to large grains sizes, polytons are expected. In sedimentary basins, for large Deborah numbers corresponding to small fluid viscosity shaggy shock waves are expected. At sufficiently large Deborah number, the limit compaction regime corresponds to polytons. Polytons are defined as a train of quasi solitary waves. They thus share some characteristics with the usual magmons. However, their length scale is smaller and their amplitude is larger. As a consequence they may play an important role in the focusing of liquids during their circulation in the upper mantle and in the crust.

[42] This study has shown the important role played by both stress and strain relaxation in the compaction process. These results are valid for a Burgers' formalism, and they can be taken as a strong motivation to tackle more consistent, but also more complex, models, such as Andrade's model.

[43] **Acknowledgments.** This manuscript has benefited from careful and much constructive review by Reid Cooper and André Revil, as well as fruitful comments by the Associate Editor Douglas Schmitt. The authors thank Neil Ribe for his comments on an earlier version of the manuscript.

References

Andrade, E. N. D. C. (1910), On the viscous flow in metals, and allied phenomena, *Proc. R. Soc. London, Ser. A*, *84*, 1–12.

Appold, M. S., and J. A. Nunn (2002), Numerical models of petroleum migration via buoyancy-driven porosity waves in viscously deformable sediments, *Geofluids*, *2*, 233–247.

Barcilon, V., and F. Richter (1986), Nonlinear waves in compacting media, *Earth Planet. Sci. Lett.*, *164*, 429–448.
Bercovici, D., Y. Ricard, and G. Schubert (2001), A two-phase model for compaction and damage 1. General theory, *J. Geophys. Res.*, *106*, 8887–8906.
Brown, A. (2000), Evaluation of possible gas microseepage mechanisms, *Am. Assoc. Pet. Geol. Bull.*, *84*, 1775–1789.
Carter, N., and S. Kirby (1978), Transient creep and semibrittle behaviour of crystalline rocks, *Pure App. Geophys.*, *116*, 807–839.
Chopra, P. (1997), High-temperature transient creep in olivine rocks, *Tectonophysics*, *279*, 93–111.
Connolly, J. A. D., and Y. Y. Podladchikov (1998), Compaction-driven fluid flow in viscoelastic rock, *Geodin. Acta*, *11*, 55–84.
Cooper, R. (2002), Seismic wave attenuation: Energy dissipation in crystalline solids, in *Plastic Deformation of Minerals and Rocks*, *Rev. Mineral. Geochem.*, vol. 51, edited by S. Karato and H.-R. Wenk, pp. 253–290, Mineral. Soc. of Am., Chantilly, Va.
Fontaine, F., M. Rabinowicz, and J. Boulegue (2003), Hydrothermal processes at Milos Island (Greek Cyclades) and the mechanisms of compaction-induced phreatic eruptions, *Stud. Appl. Math.*, *210*, 17–33.
Fowler, A., and X. Yang (1999), Pressure solution and viscous compaction in sedimentary basins, *SIAM J. Appl. Math*, *104*, 12,989–12,997.
Garofalo, F. (1965), *Fundammentals of Creep and Creep Rupture in Metals*, 258 pp., Macmillan, New York.
Green, D. H., and R. F. Cooper (1993), Dilatational anelasticity in partial melts: Viscosity, attenuation, and velocity dispersion, *J. Geophys. Res.*, *98*, 19,807–19,817.
Gribb, T. T., and R. F. Cooper (1998), Low-frequency shear attenuation in polycrystalline olivine: Grain boundary diffusion and the physical significance of the Andrade model for viscoelastic rheology, *J. Geophys. Res.*, *103*, 27,267–27,279.
Gunzburger, Y., and F. Cornet (2007), Rheological characterization of a sedimentary formation from a stress profile inversion, *Geophys. J. Int.*, *168*, 402–418.
Hirth, G., and D. Kohlstedt (1995), Experimental constraints on the dynamics of the partially molten upper mantle, *J. Geophys. Res.*, *100*, 1981–2001.
Ito, G., Y. Shen, G. Hirth, and C. Wolfe (1999), Mantle flow, melting and dehydration of the iceland mantle plume, *Earth Planet. Sci. Lett.*, *165*, 81–96.
Jackson, I., J. D. Fitz Gerald, U. H. Faul, and B. H. Tan (2002), Grain-size-sensitive seismic wave attenuation in polycristalline olivine, *J. Geophys. Res.*, *107*(B12), 2360, doi:10.1029/2001JB001225.
Joseph, D. (1990), *Fluid Dynamics of Viscoelastic Liquids, Appl. Math. Sci.*, vol. 84, 751 pp., Springer, New York.
Kaminski, E. (2006), The interpretation of seismic anisotropy in terms of mantle flow when melt is present, *Geophys. Res. Lett.*, *33*, L02304, doi:10.1029/2005GL024454.
Kaus, B., and Y. Podladchikov (2006), Initiation of localized shear zones in viscoelastoplastic rocks, *J. Geophys. Res.*, *111*, B04412, doi:10.1029/2005JB003652.
Khodakovskii, G., and M. Rabinowicz (1998), 2D modeling of melt percolation in the mantle: The role of a melt dependent mush viscosity, *Geophys. Res. Lett.*, *25*, 683–686.
Khodakovskii, G., M. Rabinowicz, G. Ceuleneer, and V. P. Trubitsyn (1995), Melt percolation in a partially molten mantle mush: Effect of a variable viscosity, *Earth Planet. Sci. Lett.*, *134*, 267–281.
Mackwell, S., D. Kohlstedt, and M. Paterson (1985), The role of water in the deformation of olivine sigle crystals, *J. Geophys. Res.*, *90*, 11,319–11,334.
McKenzie, D. (1984), The generation and compaction of partially molten rock, *J. Petrol.*, *25*, 713–765.
Miller, S. A., C. Collettini, L. Chiaraluce, M. Cocco, M. Barchi, and B. J. P. Kaus (2004), Aftershocks driven by a high-pressure CO_2 source at depth, *Nature*, *427*(6976), 724–727.
Pollitz, F. (2003), Transient rheology of the uppermost mantle beaneath the Mojave Desert, California, *Earth Planet. Sci. Lett.*, *215*, 89–104.
Post, J. R. (1977), High-temperature creep of Mt. Burnet Dunite, *Tectonophysics*, *42*, 75–110.
Rabinowicz, M., Y. Ricard, and M. Grégoire (2002), Compaction in a mantle with a very small melt concentration: Implications for the generation of carbonatitic and carbonate-bearing high alkaline mafic melt imprenations, *Earth Planet. Sci. Lett.*, *203*, 205–220.
Reiner, M. (1964), The Deborah number, *Phys. Today*, *17*, 62.
Revil, A. (2002a), The hydroelectic problem of porous rocks: thermodynamic approach and introduction of a percolation threshold, *Geophys. J. Int.*, *151*(3), 944–949.
Revil, A. (2002b), Genesis of mud volcanoes in sedimentary basins: A solitary wave-based mechanism, *Geophys. Res. Lett.*, *29*(12), 1574, doi:10.1029/2001GL014465.
Revil, A., and L. M. Cathles III (2002), Fluid transport by solitary waves along growing faults: A field example from the south Eugene Island basin, Gulf of Mexico, *Earth Planet. Sci. Lett.*, *202*, 321–335.
Revil, A., P. Leroy, A. Ghorbani, N. Florsch, and A. R. Niemeijer (2006), Compaction of quartz sands by pressure solution using a cole-cole distribution of relaxation times, *J. Geophys. Res.*, *111*, B09205, doi:10.1029/2005JB004151.
Ribe, N. (1987), Theory of melt segregation: A review, *J. Volcanol. Geotherm. Res.*, *33*, 241–253.
Ricard, Y., D. Bercovici, and G. Schubert (2001), A two-phase model for compaction and damage: 2. Application to compaction, deformation, and the role of interfacial surface tension, *J. Geophys. Res.*, *106*, 8907–8924.
Richter, F., and D. McKenzie (1984), Dynamical models for melt segregation from a deformable matrix, *J. Geol.*, *92*, 729–740.
Saenger, E. H., S. A. Shapiro, and Y. Keehm (2005), Seismic effects of viscous Biot-coupling: Finite difference simulations on micro-scale, *Geophys. Res. Lett.*, *32*, L14310, doi:10.1029/2005GL023222.
Schmeling, H. (2006), A model of episodic melt extraction for plumes, *J. Geophys. Res.*, *111*, B03202, doi:10.1029/2004JB003423.
Scott, D. (1988), The competition between percolation and circulation in a deformable porous medium, *J. Geophys. Res.*, *93*, 6451–6462.
Scott, D. R., and D. J. Stevenson (1984), Magma solitons, *Geophys. Res. Lett.*, *11*, 1161–1164.
Spiegelman, M. (1993a), Flow in deformable porous media. Part 1. Simple analysis, *Earth Planet. Sci. Lett.*, *247*, 17–38.
Spiegelman, M. (1993b), Flow in deformable porous media. Part 2. The relationship between shock waves and solitary waves, *Earth Planet. Sci. Lett.*, *247*, 39–63.
Spiegelman, M. (2003), Linear analysis of melt band formation by simple Shear, *Geochem. Geophys. Geosyst.*, *4*(9), 8615, doi:10.1029/2002GC000499.
Spiegelman, M., and P. Kelemen (2003), Extreme chemical variability as a consequence of channelized melt transport, *Geochem. Geophys. Geosyst.*, *4*(7), 1055, doi:10.1029/2002GC000336.
Spiegelman, M., and D. McKenzie (1987), Simple 2-D models for melts extraction at mid-ocean ridges and island arcs, *Earth Planet. Sci. Lett.*, *83*, 137–152.
Spiegelman, M., P. Kelemen, and E. Aharonov (2001), Causes and consequences of flow organization during melt transprot: The reaction infiltration instability in compactible media, *J. Geophys. Res.*, *106*, 2061–2077.
Suetnova, E., and G. Vasseur (2000), 1-d modelling rock compaction in sedimentary basins using a visco-elastic rheology, *Earth Planet. Sci. Lett.*, *178*, 373–383.
Vassilyev, O., Y. Podladchikov, and D. Yuen (1998), Modeling of compaction driven flow in poroelastic medium using adaptative wavelet collocation method, *Geophys. Res. Lett.*, *25*, 3239–3242.
Wiggins, C., and M. Spiegelman (1995), Magma migration and magmatic solitary waves in 3-D, *Geophys. Res. Lett.*, *22*, 1289–1292.
Yang, X.-S. (2000), Nonlinear viscoelastic compaction in sedimentary basins, *Nonlinear Proc. Geophys.*, *7*, 1–7.
Yoshino, T., M. J. Walter, and T. Katsura (2003), Core formation in planetesimals triggered by permeable flow, *Nature*, *422*, 154–157, doi:10.1038/Nature01,459.
Yuen, D., and R. Sabadini (1986), On transient rheology and glacial isostasy, *J. Geophys. Res.*, *91*, 11,420–11,438.

B. Chauveau and E. Kaminski, Équipe de Dynamique des Fluides Géologiques, Institut de Physique du Globe de Paris, 4 place Jussieu, Paris CEDEX 05, F-75252, France. (chauveau@ipgp.jussieu.fr; kaminski@ipgp.jussieu.fr)